

modeled TOARF and BOARF are -3.3 and -12 W m^{-2} , respectively. However, the annual observed TOARF and BOARF are significantly different at -10 and -52 W m^{-2} , respectively. The analysis of observed and modeled TOARF agrees with previous studies in highlighting the need for more accurate specification of surface albedo over the region. Due to the high surface albedo of the central Arabian Peninsula, mineral dust aerosols tend to warm the atmosphere in summer (June–August).

1 Introduction

Atmospheric mineral dust is a natural aerosol and is ubiquitous in the Earth's atmosphere, despite that it is emitted from hyper-arid, arid and semi-arid regions on the globe. About 2000 Mt is emitted annually to the atmosphere, 1500 Mt is deposited to the land and 500 Mt is deposited onto the ocean surface (Shao et al., 2011). It affects radiation by absorption and scattering that in turn affects surface and atmospheric temperature, also it acts as ice cloud condensation nuclei (ICCN) that impacts the microphysics of the clouds and its radiative properties (IPCC, 2013). The transported dust also carries nutrients and bacteria, which may affect the marine life and land surface life. For instance, 20 Mt of nutrients rich Saharan dust is transported to the Amazon basin in South America each year (Koren et al., 2006). Atmospheric mineral dust, especially fine dust (smaller than $2.5 \mu\text{m}$) may cause cardiopulmonary disease and lung cancer (Giannadaki et al., 2014). It also affects many of human activities like aviation, real estate construction, agriculture, and water resource management (Stefanski and Sivakumar, 2009).

Dust particles are emitted from major deserts on the globe (e.g., Sahara, the Arabian Peninsula, Taklamakan and Gobi deserts in China, Australia deserts and Atacama desert in Chile). The mineral dust emission processes (i.e., saltation and sandblasting) are determined by meteorological conditions (e.g., atmospheric instability, soil moisture). Large-scale wind systems may carry coarse and fine dust particles horizontally for thousands of kilometers (e.g., Koren et al., 2006) and vertically up 6 to 10 km (e.g.,

1525

Gobbi et al., 2004). Depending on dust particle size and atmospheric conditions dust particles may remain airborne between 1.5 to 7.4 days and will then deposit to the surface by gravitational settling or rain washout (Shao et al., 2011).

This paper focuses on atmospheric mineral dust over the Arabian Peninsula, a region, which has been less studied over the last decades compared to Saharan regions. In an early study Wilkerson (1991) described the onset and evolution of dust storms over Iraq and Kuwait analyzing satellite images and visibility records. Wilkerson's study categorized the types of dust storms as pre-frontal, post-frontal and Shamal types, the latter being a regional northwesterly wind that typically occurs in summer ("Shamal" denotes "northerly wind" in Arabic). Mashat et al. (2008) used meteorological observations from Saudi Arabia to analyze the meteorological conditions which favored dust storms and their spatial and seasonal distribution. They found that dust storms most frequently occur in the eastern part of the Arabian Peninsula in spring and extend towards the southern part of the Arabian Peninsula in summer. Alharbi (2009) and Alharbi et al. (2013) explored dust storms generation over the Arabian Peninsula, dust source regions and atmospheric conditions that promote dust storms, which include large-scale atmospheric instability, high surface winds, and dry, rich dust sources. The quantification and characterization of mineral dust aerosol (e.g., dust concentrations profile and mineral dust optical properties) became possible after the installation of The **AEROSOL ROBOTIC NET**work (AERONET) in Bahrain and Saudi Arabia around 1998. Smirnov et al. (2002) used a one year data record (July 1998–July 1999) of the Bahrain site in the Arabian Gulf to deduce the climatology of aerosol optical properties (i.e., the Aerosol Optical Depth (AOD) and the Ångström parameter). In 2004 an intensive measurement campaign was held in the United Arab Emirates (UAE), which led to the installation of various AERONET stations. Among them only the Mezaira site is fully operational up to date. This campaign characterized the nature of atmospheric aerosol over the UAE and validated satellite aerosol products over a bright surface such as desert (Reid et al., 2005; Eck et al., 2008). Kim et al. (2011) studied AERONET data records from North Africa and the Arabian Peninsula and derived the seasonal behav-

2.1.4 OMI

The Ozone Monitoring Instrument (OMI) has been orbiting the Earth on one of the EOS mission “Aura spacecraft” since July 2004. OMI is a high spatial resolution (13 km × 24 km) ground pixel size ultraviolet/visible (UV/VIS) backscatter spectrometer (Levelt et al., 2006). The OMI aerosol retrieval algorithm is the same as for the Total Ozone Mapping spectrometer (TOMS) near-UV method of aerosol absorption sensing from space (Torres et al., 2005). The accuracy of the OMI retrieval of aerosol optical depth is around 30 % relative to AERONET measurements (Torres et al., 2005).

The extinction AOD at 500 nm (near-UV) has been selected from the OMI product from Giovanni site portal (<http://Giovanni.gsfc.nasa.gov/giovanni>). From that data we selected 2° × 2° box around the three AERONET stations (see Fig. 1) for comparison purposes with the observations. The time span of this data is from January 2008 to December 2011.

2.2 Model description and experimental design

2.2.1 General model description

The International Centre for Theoretical Physics (ICTP) Regional Climate Model (RegCM) was built upon the National Center for Atmospheric Research (NCAR) Mesoscale Model version 4 (MM4) (Giorgi and Bates, 1989; Giorgi et al., 1993a, b).

The Regional Climate Model version 4 (RegCM4) is the second major development of the RegCM core after RegCM3 (Pal et al., 2007). The coding structure is completely changed. It has become totally FORTRAN 90 compliant and modular structured and its parallelization and memory management has become more efficient. The RegCM4 has more physics options, which include the Community Land surface Model (CLM3.5) land surface parameterization, the Tiedtke convection scheme, the University of Washington (UW) planetary boundary layer (PBL) scheme, and the Rapid Radiative Transfer Model (RRTM) (Giorgi et al., 2012).

1531

RegCM4 is an online climate-chemistry model and has an online gas-phase chemistry scheme (CBMZ) (Shalaby et al., 2012). It has various aerosol components such as, four size bin dust, two size bin sea salt, sulphate, black carbon and organic carbon. Sulphate, black carbon and organic carbon (Solmon et al., 2006), as well as dust and sea-salt are radiatively active (Zakey et al., 2006, 2008).

2.2.2 Dust parameterization

Sand particles are affected by many forces that determine their fate. Dust particles have three dynamic modes: (a) saltation: small particles move by jumping like leap-frog, Once lifted by wind it will drift downwind and return to hit the ground again and transfer energy and momentum to other soil aggregates (soil particles). (b) Creeping: large dust particles cannot be lifted into the air, but will just move and slide on the ground. (c) Suspension: if the upward draft is strong enough to compensate the gravitational force of the dust particles, dust will remain airborne and be transported by the wind over longer distances until its gravitational force overcome the uplifting force. It is believed that saltation is the main mechanism for surface dust emission (Shao et al., 1993; Marticorena and Bergametti, 1995).

Following Marticorena and Bergametti (1995) and Alfaro and Gomes (2001), a complex dust emission scheme has been implemented in RegCM3 (Zakey et al., 2006). This emission scheme is based on parameterization of soil aggregate saltation and sandblasting processes. According to this scheme, a critical parameter for the dust saltation process is the threshold friction velocity u_t^* , which is a function of particle size D_p (Eq. 1), such that, u_{ts}^* represents an ideal minimum threshold friction velocity, f_{eff} is a correction factor accounting for the effect of surface roughness and f_w is a factor that accounts for the effect of soil moisture content on the threshold friction velocity. The particle size is determined by the land surface soil texture. Calculating the threshold friction velocity is required to calculate the horizontal dust flux (dH_F) (Eq. 2), such that, E is the ratio of erodible to total surface, dS_{rel} is the relative surface of soil aggregate of diameter D_p to the total aggregate surface and $R(D_p)$ is the ratio of the threshold

1532

3 AOD climatology

3.1 The annual cycle

Figure 2 shows the comparison between modeled AOD and observed MISR's AOD, for seasonal average.

5 The AOD is quite variable in space and time, yet shows a clear seasonal cycle. In September–December, the model and MISR have the lowest AOD (0.1–0.3). The AOD maximum (0.3) extends from northern Iraq to the southern part of the Arabian Peninsula up to the Arabian Sea. This maximum is in the vicinity of the Arabian Gulf and Najd plateau. The model and MISR show higher AOD over the Red Sea near
10 the Bab-el-Mandab strait and parallel to the Yemen mountain ranges compared to the inland neighborhood. MISR's AOD is higher than the modeled AOD over the Arabian Sea due to the contribution of sea-salt aerosols.

In January–April, there is quite strong dust activity over the region of interest. The AOD increases over all source regions (S1, S2, S3, S4 and S5; for locations see Fig. 1a
15 with variable magnitudes. The AOD ranges from 0.3 to 0.5, the band of the highest AOD lies between the Arabian Gulf and Najd plateau. The band has a tongue shape extended inside Iraq (S1) and has a flattened base near the El Rob El khali desert (S3). The Somalia (S4) and Iran-Pakistan-Afghanistan (S5) dust sources do not contribute too much to the AOD over the entire region.

20 The model's AOD spatial distribution is quite similar to MISR, yet overestimates AOD around the S1, S2 and S5 dust sources in January–April. In April, the model and MISR results become close to each other. During February–April, the model shows systematic decrease of AOD off the southern coast of the Arabian Peninsula; however, MISR shows higher AOD over the Indian Ocean/Arabian Sea, which may be attributed to sea
25 salt aerosol.

In the May–August months the AOD reaches its maximum (0.5–0.9). In May the maximum AOD band is between the Arabian Gulf and Najd Plateau. This band migrates

1535

southward south in July–August. The AOD over the Red Sea and the Gulf of Aden increases steadily and reaches its maximum in July.

The model shows a comparable spatial distribution, yet overestimates AOD values. The modeled AOD maximum is centered over El Rob El khali desert (S3) in the south-
5 eastern Arabian Peninsula. The AOD spatial distribution is controlled mainly by the topography of the region. The eastern Arabian Gulf high land that extends from the Anatolia plateau in Turkey to southern Iran parallel to the Arabian Gulf (Fig. 1b) and the Najed Plateau in the central Arabian Peninsula (Fig. 1b) act as a funnel that controls the wind flow system in that complex region. The MISR AOD shows such a banana-
10 like shape for the spatial distribution of maximum AOD; model's AOD shows this shape to a certain extent. In June, July and August, the model underestimates the AOD in the northern part of the Peninsula especially in Iraq, Jordan and Kuwait. However, the model overestimates AOD in the southeastern part of the Arabian Peninsula over Yemen, Oman and UAE.

15 The analysis of the annual cycle of the zonally averaged AOD reveals interesting features of the temporal AOD development across the domain. Figure 3a represents the zonally averaged AOD (36–50° E) and the area of interest spans from 10–30° N. The model shows a first maximum in March and April centered at 25° N, the model's AOD decreases in April and start to increase again in May. The second maximum is in
20 mid-summer (July) and centered between 10 and 20° N. This second maximum reveals two peaks: one represents the southern Arabian Peninsula dust sources (15–20° N) and the other one the Somalia dust sources (10–15° N); the minimum in between is the Bab-Elmandab strait and Gulf of Aden.

25 The MISR annual cycle of the zonally averaged AOD shows a bit different distribution (Fig. 3b). The first maximum is in between April and May and is centered at 28° N. The second maximum is in July and is centered between 10 and 20° N. It has two peaks, however they are not clear as MISR, one represents the Arabian Peninsula dust sources and the other represents the Somalia dust sources. The analysis of the large-scale circulation provides a plausible explanation of such a bi-modal behavior.

1536

dust sources in northern Arabia. There are two types of frontal type dust, pre-frontal type and post-frontal type (Wilkerson, 1991). The frontal system is associated with instability of the air column, which results in dust uplifting. The summertime dust storm is a result of strong north to northwest wind associated with the Indian monsoon depression.

4.1 Spring time (cold season)

4.1.1 Large-scale circulation

In winter and early spring (January–April) the Arabian Peninsula is affected by an extension of Siberian High pressure and the Red Sea trough in northern part and southern part of the Arabian Peninsula respectively. The anti-cyclonic wind field is dominated over the Arabian Peninsula. Figure 7a and b shows the climatology of the mean sea level pressure (MSLP), while Fig. 7d and e shows the climatology of temperature and wind field at 850 hPa geopotential surface. While the extension of Siberian high pressure with cold air mass affects the northern part of the Arabian Peninsula (Fig. 7a and b), the southerly winds which are associated with the Red Sea trough over the southern Arabian Peninsula advect warm air toward north (Fig. 7d and e), which leads to instabilities in the atmosphere.

The position and strength of the Sub-Tropical Jet (STJ) at 200 hPa determine the atmospheric stability at the surface. Figure 7g and h shows the climatology of the STJ. In winter the STJ core is located over the Arabian Peninsula. The spring STJ core is weaker than the winter STJ. It migrates toward north in April–May and displays a strong meridional component (Fig. 7g and h). Alhabri et al. (2013) described the role of the STJ in the onset and development of dust storms. Briefly, the STJ generates regions of upward motion and downward motion (i.e. secondary circulation). The north side of the STJ core is a divergence zone that is associated with upward motion, while the south of the STJ core is a convergence zone that is associated with downward motion. Figure 8 shows the zonally averaged vertical velocity (Ω in hPa s^{-1} where

1541

(–) values designate upward motion and (+) values designate downward motion). In December–April the STJ core is located south of 30°N (Fig. 7g and h), and Fig. 8 shows the secondary circulation region of upward motion and downward motion from surface (1000 hPa) to the upper air (100 hPa) south of 30°N . In late winter (February) and spring time (March–April) the upward motion progressively strengthens from 20°N to 30°N and from surface to upper air levels.

In most part of the Arabian Peninsula, the prevailing wind directions are southerlies and southwesterlies. The observations over the northern and southern parts of the Arabian Peninsula show that during the dust season, the prevailing wind directions are southerlies and southwesterlies (Mashat et al., 2008). Figure 9 shows the climatology of the zonally averaged wind's meridional component. The southerly meridional component shows the ascending motion and the sliding of warm air over the cold air from the north.

Figure 10 shows the climatology of the zonally averaged vertical profile of fine dust concentration. The maximum concentration is located between 15 and 30°N . The dust concentrations progressively increase towards north from December to February and start to retreat in April. In winter and spring, dust layers do not extend to high levels in the atmosphere, actually they are confined to levels below 800 hPa.

4.1.2 Land surface response

The friction velocity is the sole dynamical variable in the dust parameterization (the other variables are land surface characteristics). The land surface response of the large scale circulation is reflected by the friction velocity. Also, according to Eqs. (2) and (3), the dust emission is proportional to the friction velocity. In Supplement Fig. S1 the friction velocity over land surfaces is shown and in the following discussion, we will focus in particular on the dust source regions (Fig. 1a).

In the late winter and early spring months (January–March) the friction velocity is high in the western and central part of the Arabian Peninsula (Fig. S1). Correspondingly, dust emissions are also higher in the western and central Arabian Peninsula com-

1542

pared to the surrounding areas (Fig. 11). Over the source region S4 (Al Roub AL khali desert) dust emission is clearly accompanied with high friction velocity. In the northern part of the Arabian Peninsula the climatology of the friction velocity does not reflect the abovementioned relation between friction velocity and surface dust emission. Although,

5 this region is affected by a high pressure system which causes a weak surface wind field, most of the emitted dust in this region is due to a fast migrating cyclone over the Syria–Iraq area associated with high surface wind (Mashat et al., 2008; Abdi Vishkaee et al., 2012; Alharbi et al., 2013) that has been filtered out in the averaging procedure.

10 The corresponding atmospheric surface dust concentration for dust less than $10\ \mu\text{m}$ is shown in Fig. S2. In the months from December to April the surface dust concentration over the Arabian Peninsula reaches up to $120\ \mu\text{g m}^{-3}$ in the central region, which is in agreement with results for the same region performed in a global modeling study by Ginoux et al. (2004).

4.2 Summer time (warm season)

15 4.2.1 Large-scale circulation

Starting mid-spring (i.e. April) the surface high pressure retreats and the Indian Monsoon depression starts to progress towards the Arabian Peninsula. In summer (June–August) the Arabian Peninsula is largely impacted by the Indian Monsoon depression and it further intensifies during summer months (Fig. 7c). The prevailing winds in this

20 season are northerlies and northwesterlies (“Shamal”) over the most of the Arabian peninsula (Mashat et al., 2008), while the southern part is affected by strong southerly winds associated with the Low-Level Jet (i.e. Somalia Jet) that is triggered by the Indian Monsoon (Fig. 7f). In late spring and summer (i.e. April–August), the STJ migrates toward north and a high pressure is develops over the Arabian Peninsula (Fig. 7i).

25 The summer meridional components in Fig. 9 become northerly, which is an indication of the Indian Monsoon cyclonic circulation. In addition, Fig. 8 shows that the ascending motion in the southern part of the Arabain Peninsula ($15\text{--}25^\circ\text{N}$) is higher

1543

than during the winter-spring time. The descending motion over the ocean is evident in the summer season at latitudes from 10 to 15°N . According to Fig. 10 the ascending motion in southern Arabia in upper air results in uplifting of dust to higher atmospheric levels up to the $500\ \text{hPa}$ level. After the retreat of the Indian Monsoon, the ascending motion weakens significantly and the meridional velocity reverses its sign to be

5 southerly again.

4.2.2 Land surface response

During the summer season, starting June, the friction velocity (Fig. S1) gets higher in the eastern and southern part of the Arabian Peninsula, and over Somalia (dust sources S3 and S4 in Fig. 1a). As a consequence high surface dust emission fluxes (Fig. 11) occur over the eastern and the southern Arabian Peninsula (e.g. in Oman) and over Somalia. Those source regions contribute significantly to the resultant AOD in summer. The surface dust concentration in summer reaches maximum values between $100\text{--}180\ \mu\text{g m}^{-3}$ (Fig. S2).

15 5 Dust radiative impact

The ultimate aim of studying the climatology of aerosol in any climate chemistry model like RegCM4 is to estimate the radiative feedback of aerosol on climate (Stanelle et al., 2010), namely, the radiative forcing of the aerosol. With regard to some Global Climate Model (GCM) simulations, the principal radiative effect of mineral dust is heating the

20 atmosphere in the source region. This results in inhibiting convection and reduction in precipitation (Tegan and Lacis, 1996). The analysis of radiative forcing and its dependence on particle size shows that regardless of the particle size dust particles exert negative radiative forcing (cooling effect) near the Earth’s surface. However, such negative radiative forcing decreases with height according to the dust particle’s radius. The radiative forcing becomes positive (heating effects) for larger particle at higher levels

25

1544

Figure S4 displays the seasonal evolution of TOARF. There are pronounced negative values over the sea surface, but, over land surface the TOARF signal is close to zero or may even become positive over the center of the Arabian Peninsula especially in July. This feature is related to the underlying land surface albedo, where the Arabian Peninsula has a higher surface albedo that contributes to TOARF.

6 Summary and conclusions

The Regional Climate Model version 4 (RegCM4) has been used to simulate the occurrence and distribution of atmospheric mineral dust aerosol over the Arabian Peninsula. Thirteen years of high resolution simulation and a comparison with a suite of observational datasets were utilized to understand the climatology of atmospheric dust occurrence. Observational data included Kuwait University, Solar-Village and UAE-Mezaira AERONET stations, having the longest AOD record, and satellite AOD retrievals from MISR, OMI and MODIS (Deepblue) from 2006 to 2012.

While the modeled AOD shows that the dust season extends from March to August with two pronounced maxima, one over the northern Arabian Peninsula in March (AOD ≈ 0.4) and one over the southern Arabian Peninsula in July (AOD ≈ 0.7), the observations indicate a dust season, which extends from April to August with two pronounced maxima, one over the northern Arabian Peninsula in April (AOD ≈ 0.5) and one over the southern Arabian Peninsula in July (AOD ≈ 0.5). The zonally averaged annual cycle AOD analysis shows two AOD peaks, one in springtime (March–May) and one in summertime (June–August). While the model and the observations agree in the timing of the summertime peak, there is some disagreement in the springtime peak where the model reveals a springtime peak about, one month earlier (February–March). This bi-modal oscillation of dust occurrence is caused by the large scale circulation and the land surface response.

In spring the Arabian Peninsula is under the influence of the Siberian high from the north and north-east and the extension of the Red Sea trough from the south and

1547

south-west. The frontal area between the cold air in the north and warm air in the south promotes a strong southerly wind with enhanced upward motion, which results in dust uplifting in the northern and western part of the Arabian Peninsula. This is favored by increased surface friction in these areas at the same time.

In summer the atmospheric circulation entirely changes. The Arabian Peninsula is affected by the extension of Indian Monsoon Depression that causes the Shamal, a strong northwesterly wind aligned along the Arabian Gulf. The Shamal is strong enough to push and concentrate dust over the southern part of the Arabian Peninsula. At the same time the Somalia Low-Level Jet strongly enhances the dust uplifting from dust sources in Somalia. The Somalia dust contributes significantly to the overall dust burden over the region, especially over the Red and Arabian Sea.

The Top of Atmosphere Radiative Forcing (TOARF) and the Bottom of Atmospheric Radiative Forcing (BOARF) data retrieved from AERONET were used to analyze the atmospheric dust radiative forcing to obtain a better understanding of potential climate feedback mechanisms in the region. While the model captures the annual cycle of TOARF and BOARF, it underestimates both by a factor of 3 and 4, respectively. These biases contribute to the large uncertainty of modeled surface temperature over the Arabian Peninsula noticed earlier by Steiner et al. (2014).

Overall, the seasonal behavior of BOARF shows a negative radiative forcing with a maximum in the summer (cooling effects) over the whole domain and with maximum negative radiative forcing over the Arabian Peninsula and Somalia compared to other regions with relatively high dust concentration like Pakistan or the Caspian Sea region. Our study indicates that this is due to the fact that dust in those regions does not extend to upper air like it is the case over the Arabian Peninsula.

The model's TOARF is less negative and may even display some positivity in the central region of the Arabian Peninsula. The analysis of the observed and modeled TOARF shows that, it is essential to consider the surface albedo of the region. With the high surface albedo of the central Arabian Peninsula, mineral dust aerosols tend to warm the atmosphere in summer (June–August).

Acknowledgements. We gratefully acknowledge the data provided by the AERONET network and we wish to express our appreciation to the operators of stations for maintaining these important measurements.

References

- Abdou, W. A., Diner, D. J., Martonchik, J. V., Bruegge, C. J., Kahn, R. A., Gaitley, B. J., Crean, K. A., Remer, L. A., and Holben, B.: Comparison of coincident multiangle imaging spectroradiometer and moderate resolution imaging spectroradiometer aerosol optical depths over land and ocean scenes containing aerosol robotic network sites, *J. Geophys. Res.*, 110, D10S07, doi:10.1029/2004JD004693, 2005.
- Abdi Vishkaee, F., Flamant, C., Cuesta, J., Oolman, L., Flamant, P., Khalesifard, H.: Dust transport over Iraq and northwest Iran associated with winter shamal: a case study, *J. Geophys. Res.*, 117, D03201, doi:10.1029/2011JD016339, 2012.
- Alfaro, S. C., and Gomes, L.: Modeling mineral aerosol production by wind erosion: emission intensities and aerosol size distribution in source areas, *J. Geophys. Res.*, 106, 18075–18084, 2001.
- Alharbi, B. H.: Airborne dust in Saudi Arabia: source areas, entrainment, simulation and composition, PhD dissertation, Monash university, Melbourne, Australia, 313 pp., 2009.
- Alharbi, B. H., Maghrabi, A., and Tapper, N.: The march 2009 dust event in Saudi Arabia: precursor and supportive environment, *B. Am. Meteorol. Soc.*, 94, 515–528, 2013.
- Dee, D. P., Uppala, S. M., Simmons, A. J., Berrisford, P., Poli, P., Kobayashi, S., Andrae, U., Balmaseda, M. A., Balsamo, G., Bauer, P., Bechtold, P., Beljaars, A. C. M., Van de Berg, L., Bidlot, J., Bormann, N., Delsol, C., Dragani, R., Fuentes, M., Geer, A. J., Haimberger, L., Healy, S. B., Hersbach, H., Hólm, E. V., Isaksen, I., Kållberg, P., Köhler, M., Matricardi, M., McNally, A. P., Monge-Sanz, B. M., Morcrette, J.-J., Park, B.-K., Peubey, C., de Rosnay, P., Tavolato, C., Thépaut, J.-N., and Vitart, F.: The ERA-interim reanalysis: configuration and performance of the data assimilation system, *Q. J. Roy. Meteor. Soc.*, 137, 553–597, 2011.
- Dickinson, R. E., Henderson-Sellers, A., and Kennedy, P. J.: Biosphere–atmosphere transfer scheme version 1e as coupled to the NCAR community climate model, Tech. Rep., National Center for Atmos. Res., Boulder, Colorado, USA, 1–80, 1993.
- Diner, D. J., Beckert, J. C., Reilly, T. H., Bruigge, C. J., Conel, J. E., Kahn, R. A., Martonchik, J. V., Acherman, T. P., Davies, R., Gerstl, S. A. W., Gordon, H. R., Muller, J., Myrneni, R. B., Sellers, P. J., Pinty, B., and Verstraete, M. M.: Multi-angle imaging spectroradiometer (misr) instrument description and experiment overview, *IEEE T. Geosci. Remote*, 36, 1072–1087, 1998.
- Dubovik, O. and King, M. D.: A flexible inversion algorithm for retrieval of aerosol optical properties from Sun and sky radiance measurements, *J. Geophys. Res.*, 105, 20673–20696, 2000.
- Eck, T. F., Holben, B. N., Reid, J. S., Sinyuk, A., Dubovik, O., Smirnov, A., Giles, D., O'Neill, N. T. N., Tsay, S.-C., Ji, Q., Mandoos, A. A., Khan, M. R., Reid, E. A., Schafer, J. S., Sorokine, M., Newcomb, W., and Slusker, I.: Spatial and temporal variability of column-integrated aerosol optical properties in the southern Arabian Gulf and United Arab Emirates in summer, *J. Geophys. Res.*, 113, D01204, doi:10.1029/2007JD008944, 2008.
- Emmons, L. K., Walters, S., Hess, P. G., Lamarque, J.-F., Pfister, G. G., Fillmore, D., Granier, C., Guenther, A., Kinnison, D., Laepple, T., Orlando, J., Tie, X., Tyndall, G., Wiedinmyer, C., Baughcum, S. L., and Kloster, S.: Description and evaluation of the model for ozone and related chemical tracers, version 4 (MOZART-4), *Geosci. Model Dev.*, 3, 43–67, 2010.
- García, O. E., Díaz, J. P., Expósito, F. J., Díaz, A. M., Dubovik, O., Derimian, Y., Dubuisson, P., and Roger, J.-C.: Shortwave radiative forcing and efficiency of key aerosol types using AERONET data, *Atmos. Chem. Phys.*, 12, 5129–5145, doi:10.5194/acp-12-5129-2012, 2012.
- Giannadaki, D., Pozzer, A., and Lelieveld, J.: Modeled global effects of airborne desert on air quality and premature mortality, *Atmos. Chem. Phys.*, 14, 957–968, doi:10.5194/acp-14-957-2014, 2014.
- Giorgi, F. and Bates, G. T.: The climatological skill of a regional model over complex terrain, *Mon. Weather Rev.*, 117, 2325–2347, 1989.
- Giorgi, F., Bates, G. T., and Nieman, S. J.: The multi-year surface climatology of a regional atmospheric model over the western United States, *J. Climate*, 6, 75–95, 1993a.

- Giorgi, F., Marinucci, M. R., and Bates, G. T.: Development of a second generation regional climate model (regcm2) i: boundary layer and radiative transfer processes, *Mon. Weather Rev.*, 121, 2794–2813, 1993b.
- Giorgi, F., Coppola, E., Solmon, F., Mariotti, L., Sylla, M. B., Bi, X., Elguindi, N., Diro, G. T., Nair, V., Giuliani, G., Turuncoglu, U. U., Cozzini, S., Guttler, I., O'Brien, T. A., Tawfik, A. B., Shalaby, A., Zakey, A. S., Steiner, A. L., Stordal, F., Sloan, L. C., and Brankovic, C.: RegCM4: model description and preliminary tests over multiple CORDEX domains, *Clim. Res.*, 52, 7–29, doi:10.3354/cr01018, 2012.
- 5 Ginoux, P., Prospero, J. M., Torres, O., and Chin, M.: Long term simulation of global dust distribution with the GOCART model: correlation with north Atlantic oscillation, *Environ. Modell. Softw.*, 19, 113–128, 2004.
- 10 Gobbi, G. P., Barnaba, F., and Ammannato, L.: The vertical distribution of aerosols, Saharan dust and cirrus clouds in Rome (Italy) in the year 2001, *Atmos. Chem. Phys.*, 4, 351–359, 2004, <http://www.atmos-chem-phys.net/4/351/2004/>.
- 15 Grell, G.: Prognostic evaluation of assumptions used by cumulus parameterization, *Mon. Weather Rev.*, 121, 764–787, 1993.
- Hillel, D.: Introduction to environmental soil physics, Academic Press, Massachusetts, USA, 494 pp., 2003.
- 20 Holben, B. N., Eck, T. F., Slutsker, I., Tanre, D., Buis, J. P., Setzer, A., Vermote, E., Reagan, J. A., Kaufman, Y. J., Nakajima, T., Lavenu, F., Jankowiak, I., and Smirnov, A.: AERONET A federated Instrument network and data archive for aerosol characterization, *Remote Sens. Environ.*, 66, 1–16, 1998.
- IPCC: Climate Change 2013: The Physical Basis. Contribution of Working Group I to the Fifth Assessment Report of the Intergovernmental Panel on Climate Change, edited by: Stocker, T. F., Qin, D., Plattner, G.-K., Tignor, M., Allen, S. K., Boschung, J., Nauels, A., Xia, Y., Bex, V., and Midgley P. M., Cambridge University Press, Cambridge, United Kingdom and New York, USA, 1535 pp., 2013.
- 25 Kalenderski, S., Stenchikov, G., and Zhao, C.: Modeling a typical winter-time dust event over the Arabian Peninsula and the Red Sea, *Atmos. Chem. Phys.*, 13, 1999–2014, doi:10.5194/acp-13-1999-2013, 2013.
- 30 Kiehl, J. T., Hack, J. J., Bonan, G. B., Boville, B. A., Breigleb, B. P., Williamson, D., and Rasch, P.: Description of the NCAR community climate model (CCM3), Tech. Rep.

- NCAR/TN-420+STR, National Center for Atmospheric Research, Boulder, Colorado, USA, 1–159, 1996.
- Kim, D., Chin, M., Yu, H., Eck, T. F., Sinyuk, A., Smirnov, A., and Holben, B. N.: Dust optical properties over North Africa and Arabian Peninsula derived from the AERONET dataset, *Atmos. Chem. Phys.*, 11, 10733–10741, doi:10.5194/acp-11-10733-2011, 2011.
- 5 Konarè, A., Zakey, A. S., Solmon, F., Giorgi, F., Rausher, S., Ibrah, S., and Bi, X.: A regional climate modeling study of the effect of desert dust on the west African monsoon, *J. Geophys. Res.*, 113, D12206, doi:10.1029/2007JD009322, 2008.
- 10 Koren, I., Kaufman, Y. J., Washington, R., Todd, M. C., Rudich, Y., Martins, J. V., and Rosenfeld, D.: The bodélé depression: a single spot in the Sahara that provides most of the mineral dust to the Amazon forest, *Environ. Res. Lett.*, 1, 014005, doi:10.1088/1748-9326/1/1/014005, 2006.
- Levelt, P. F., Hilsenrath, E., Leppelmeier, G. W., van den Oord G. H. J., Bhartia, P. K., Tamminen, J., de Haan, J. F., and Veefkind, J. P.: Science objectives of the ozone monitoring instrument, *IEEE T. Geosci. Remote*, 44, 1199–1208, 2006.
- 15 Marcella, M. P. and Eltahir, E. A. B.: Effects of mineral aerosols on the summertime climate of southwest Asia: incorporating subgrid variability in a dust emission scheme, *J. Geophys. Res.*, 115, D18203, doi:10.1029/2010JD014036, 2010.
- 20 Marcella, M. P. and Eltahir, E. A. B.: The role of lateral boundary conditions in simulations of mineral aerosols by a regional climate model of southwest Asia, *Clim. Dynam.*, 38, 109–120, doi:10.1007/s00382-010-0992-y, 2011.
- Marcella, M. P. and Eltahir, E. A. B.: Modeling the summertime climate of southwest Asia: the role of land surface processes in shaping the climate of semiarid regions, *J. climate*, 25, 704–719, 2012.
- 25 Marchand, R., Ackerman, T., Smyth, M., and Rossow, W. B.: A review of cloud top height and optical depth histograms from MISR, ISCCP, and MODIS, *J. Geophys. Res.*, 115, D16206, doi:10.1029/2009JD013422, 2010.
- 30 Marey, H. S., Gille, J. C., El-Askary, H. M., Shalaby, E. A., and El-Reay, M. E.: Aerosol climatology over Nile Delta based on MODIS, MISR and OMI satellite data, *Atmos. Chem. Phys.*, 11, 10637–10648, doi:10.5194/acp-11-10637-2011, 2011.
- Martcorena, B. and Bergametti, G.: Modeling the atmospheric dust cycle: 1. design of a soil-derived dust emission scheme, *J. Geophys. Res.*, 100, 16415–16430, 1995.

- Martonchik, J. V., Diner, D. J., Kahn, R., Acherman, T. P., Verstraete, M. M., Pinty, B., and Gordon, H. R.: Techniques for the retrieval of aerosol properties over land and ocean using multiangle imaging, *IEEE T. Geosci. Remote*, 36, 1212–1227, 1998.
- Martonchik, J. V., Diner, D. J., Kahn, R., Gaitley, B., and Holben, B. N.: Comparison of MISR and AERONET aerosol optical depth over desert sites, *Geophys. Res. Lett.*, 31, L16102, doi:10.1029/2004GL019807, 2004.
- Mashat, A. S., Alamodi, A. O., and Ahmed, H. A. M.: Diagnostic and prognostic study for dust (sand) storms over Saudi Arabia, Tech. Rep. V18_AR-26–89, King Abdulaziz University, Faculty of Meteorology, Environment and Arid Land Agriculture, Saudi Arabia, 2008.
- Napat, P., Solmon, F., Mallet, M., Kok, J. F., and Somot, S.: Dust emission size distribution impact on aerosol budget and radiative forcing over the Mediterranean region: a regional climate model approach, *Atoms. Chem. Phys.* 12, 10545–10567, doi:10.5194/acp-12-10545-2012, 2012.
- Nazrul Islam, M. and Almazroui, M.: Direct effect and feedback of desert dust on the climate of the Arabian Peninsula during the wet season: a regional climate model study, *Clim. Dynam.*, 39, 2239–2250, doi:10.1007/s00382-012-1293-4, 2012.
- O'Brien, T. A., Chuang, P. Y., Sloan, L. C., Faloona, I. C., and Rossiter, D. L.: Coupling a new turbulence parameterization to RegCM adds realistic stratocumulus clouds, *Geosci. Model Dev.*, 5, 989–1008, doi:10.5194/gmd-5-989-2012, 2012.
- Pal, J. S., Giorgi, F., Bi, X., Elguindi, N., Solmon, F., Gao, X., Rauscher, S. A., Francisco, R., Zakey, A., Winter, J., Ashfaq, M., Syed, F. S., Bell, J., Diffenbaugh, N., Karmacharya, J., Martinez, D., Darocha, R. P., Sloan, L. C., and Steiner, A.: Regional climate modeling for the developing world, *B. Am. Meteorol. Soc.*, 88, 1395–1409, 2007.
- Pinty, B., Taberner, M., Haemmerle, V. R., Paradise, S. R., Vermote, E., Verstraete, M. M., Gobron, N., and Widlowski, J.: Global-scale comparison of MISR and MODIS land surface model, *J. Climate.*, 24, 732–749, 2011.
- Reid, J. S., Piketh, S. J., Kahn, R., Bruintjes, R. T., and Holben, B. N.: A summary of first year activities of the United Arab Emirates unified aerosol experiment: UAE², Naval Research Laboratory, NRL/MR/7534–05-8899, Monterey, CA, USA, 2005.
- Remer, L. A., Kaufman, Y. J., Tanre, D., Mattoo, S., Chu, D. A., Martins, J. V., Li, R.-R., Ichoku, C., Levy, R. C., Kleidman, R. G., Eck, T. F., Vermote, E., and Holben, B. N.: The MODIS aerosol algorithm, products, and validation, *J. Atmos. Sci.*, 62, 947–973, 2005.

1553

- Schmid, B., Michalsky, J., Halthore, R., Beauharnois, M., Harrison, L., Livingston, J., Russell, P., Holben, B., Eck, T., and Smirnov, A.: Comparison of aerosol optical depth from four solar radiometers during the fall 1997 ARM intensive observation period, *Geophys. Res. Lett.*, 26, 2725–2728, 1999.
- Shalaby, A., Zakey, A. S., Tawfik, A. B., Solmon, F., Giorgi, F., Stordal, F., Sillman, S., Zaveri, R. A., and Steiner, A. L.: Implementation and evaluation of online gas-phase chemistry within a regional climate model (RegCM-CHEM4), *Geosci. Model Dev.*, 5, 741–760, 2012.
- Shao, Y., Raupach, M. R., and Findlater, P. A.: Effect of saltation bombardment on the entrainment of dust by wind, *J. Geophys. Res.*, 98, 12719–12726, 1993.
- Shao, Y., Wyrwoll, K., Chappell, A., Huang, J., Lin, Z., Mctainsh, G. H., Mikami, M., Tanaka, T. Y., Wang, X., and Yoon, S.: Dust cycle: an emerging core theme in earth system science, *Aeolian Res.*, 2, 181–204, 2011.
- Smirnov, A., Holben, B. N., Dubovik, O., O'Neil, N. T., Eck, T. F., Westphal, D. L., Goroch, A. K., Pietras, C., and Slutsker, I.: Atmospheric aerosol optical properties in the Persian gulf, *J. Atmos. Sci.*, 59, 620–634, 2002.
- Solmon, F., Giorgi, F., and Lioussé, C.: Aerosol modeling for regional climate studies: application to anthropogenic particles and evaluation over a European/African domain, *Tellus B Chem. Phys. Meteorol.*, 58, 51–72, 2006.
- Solmon, F., Mallet, M., Elguindi, N., Giorgi, F., Zakey, A., and Konare, A.: Dust aerosol impact on regional precipitation over western Africa: mechanisms and sensitivity to absorption properties, *Geophys. Res. Lett.*, 35, L24705, doi:10.1029/2008GL035900, 2008.
- Solmon, F., Elguindi, N., and Mallet, M.: Radiative and climatic effects of dust over west Africa as simulated by a regional climate model, *Clim. Res.*, 52, 97–113, doi:10.3354/cr01039, 2012.
- Stanelle, T., Vogel, B., Vogel, H., Baumer, D., and Kottmeier, C.: Feedback between dust particles and atmospheric processes over west Africa during dust episodes in March 2006 and June 2007, *Atmos. Chem. Phys.*, 10, 10771–10788, doi:10.5194/acp-10-10771-2010, 2010.
- Steiner, A. L., Tawfik, A. B., Shalaby, A., Zakey, A. S., Abdel-Wahab, M. M., Salah, Z., Solmon, F., Sillman, S., and Zaveri, R. A.: Climatological Simulations of Ozone and atmospheric aerosols in Greater Cairo region, *Clim. Res.*, 59, 207–228, doi:10.3354/cr01211, 2014.
- Stefanski, R. and Sivakumar, M. V. K.: Impact of sand and dust storms on Agriculture and potential agricultural application of a SDSWS, *IOP C. Ser. Earth Env.*, 7, 012016, doi:10.1088/1755-1307/7/1/012016, 2009.

1554

- Tawfik, A. B. A., and Steiner, L.: The role of soil ice in land atmosphere coupling over the United States: a soil moisture-precipitation winter feedback mechanism, *J. Geophys. Res.*, 116, D02113, doi:10.1029/2010JD014333, 2011.
- Tegan, I. and Laci, A. A.: Modeling of particle size distribution and its influences on the radiative properties of mineral dust aerosol, *J. Geophys. Res.*, 101, 19237–19244, 1996.
- 5 Torres, O., Bhartia, P. K., Sinyuk, A., Welton, E. J., and Holben, B.: Total Ozone Mapping spectrometer measurements of aerosol absorption from space: comparison to SAFARI 2000 ground-based observations, *J. Geophys. Res.*, 110, D10S18, doi:10.1029/2004JD004611, 2005.
- 10 Wilkerson, W. D.: Dust and sand forecasting in Iraq and adjoining countries, Tech. Rep. AWS/TN-91/001, Air Weather Service, Scott Air Force Base, Illinois, USA, 1991.
- Woodward, S.: Modeling the atmospheric life cycle and radiative impact of mineral dust in the Hadley Centre climate model, *J. Geophys. Res.*, 106, 18155–18166, 2001.
- Zakey, A. S., Solmon, F., and Giorgi, F.: Implementation and testing of a desert dust module in a regional climate model, *Atmos. Chem. Phys.*, 6, 4687–4704, 2006,
- 15 <http://www.atmos-chem-phys.net/6/4687/2006/>.
- Zakey, A. S., Giorgi, F., and Bi, X.: Modeling of sea salt in a regional climate model: fluxes and radiative forcing, *J. Geophys. Res.*, 113, D14221, doi:10.1029/2007JD009209, 2008.
- 20 Zhang, D. F., Zakey, A. S., Gao, X. J., Giorgi, F., and Solmon, F.: Simulation of dust aerosol and its regional feedbacks over east Asia using a regional climate model, *Atmos. Chem. Phys.*, 9, 1095–1110, 2009, <http://www.atmos-chem-phys.net/9/1095/2009/>.

1555

Table 1. Monthly deviation in [%] from the AOD annual average median for each site. Bold numbers indicate values with deviations of at least +20 % from the AOD annual average median and are considered dust season.

	AERO			MODIS			MISR			OMI			MODEL		
	Kuwait	SOLAR	UAE	Kuwait	SOLAR	UAE	Kuwait	SOLAR	UAE	Kuwait	SOLAR	UAE	Kuwait	SOLAR	UAE
Annual median	0.40	0.27	0.32	0.47	0.34	0.30	0.42	0.44	0.43	0.63	0.51	0.42	0.23	0.33	0.37
Jan	-51	-55	-42	-25	-33	-48	-46	-33	-37	-38	-31	-26	-42	-28	-42
Feb	-26	-26	-23	1	-8	-28	-7	-7	-32	-4	2	-11	2	-9	-23
Mar	-10	-0.3	-16	-2	2	-16	-14	-1	-17	0.3	13	-4	17	24	11
Apr	25	23	22	44	56	12	47	28	12	38	29	5	56	28	15
May	51	52	24	46	42	7	65	33	31	23	30	20	26	18	7
Jun	47	38	37	38	36	53	39	48	33	37	23	41	17	26	17
Jul	40	23	52	-2	6	78	24	7	58	16	17	49	37	65	82
Aug	10	32	34	-24	11	56	1	20	55	2.9	-1	21	15	55	123
Sep	-9	10	5	-25	3	-2	-17	1	-2	-3	3	-9	-25	-25	-23
Oct	-3	-15	-14	6	-27	-32	-11	-26	-31	-4	-13	-18	-41	-59	-62
Nov	-22	-34	-38	-15	-36	-37	-27	-31	-31	-30	-33	-31	-35	-52	-55
Dec	-52	-48	-41	-26	-53	-41	-53	-39	-38	-37	-39	-38	-30	-42	-50

1556

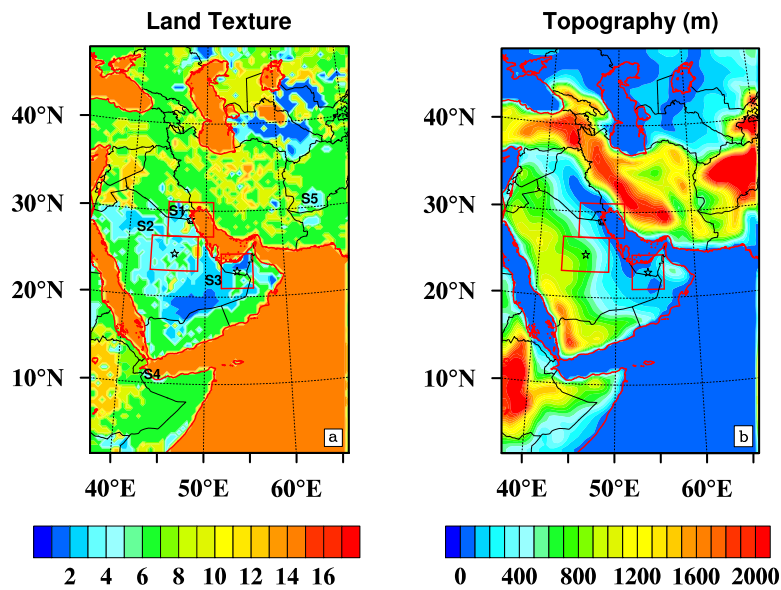


Figure 1. (a) The BATS land texture categories; (b) the topography height in meter. Stars indicate the location of the AERONET stations. All area average calculations are done for the areas surrounded by red rectangles. For detailed description of the BATS land texture categories see Zakey et al. (2006).

1559

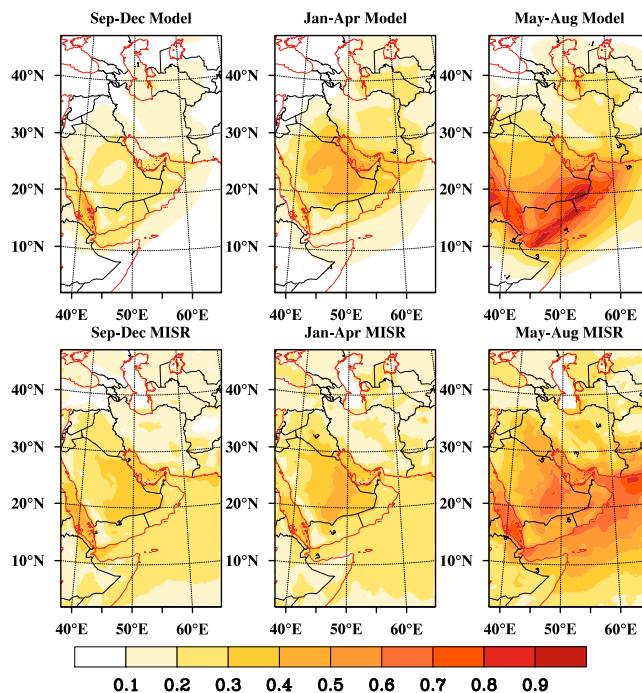


Figure 2. AOD seasonal average of 13 year of RegCM4 simulation versus MISR observations. For each season the upper panels show modeled AOD and the lower panels show MISR's observed AOD. The legend indicates the AOD.

1560

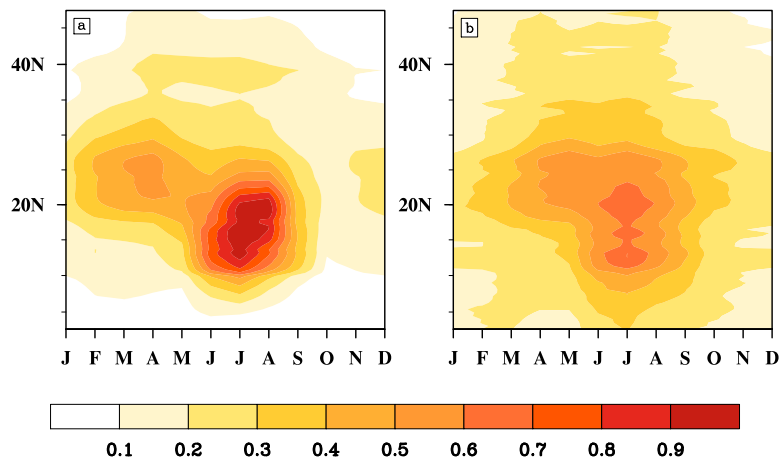


Figure 3. The annual cycle of the zonally averaged AOD (averaged from 44 to 56° E and over the 13 year simulation period), (a) RegCM4.4 AOD, (b) MISR AOD.

1561

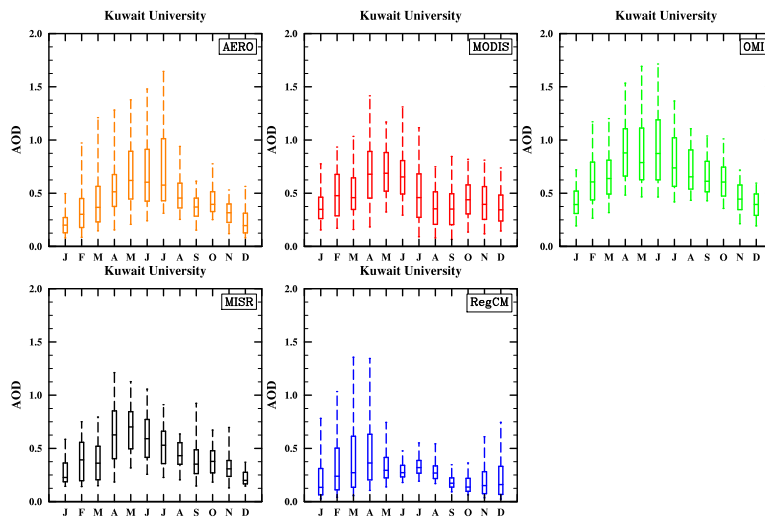


Figure 4. The AOD annual cycle statistics (5 percentile, 20 percentile, median, 75 percentile, 95 percentile) of AERONET, MODIS (deep-blue), OMI, MISR and RegCM for Kuwait University site, Kuwait.

1562

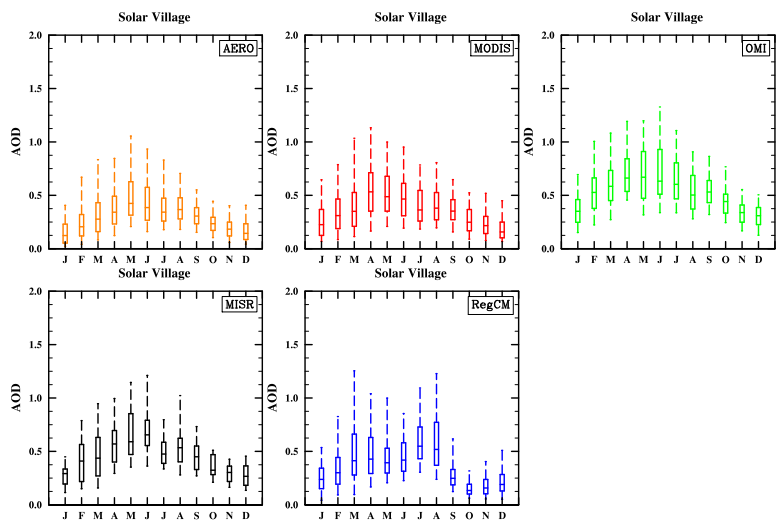


Figure 5. The AOD annual cycle statistics as in Fig. 4 but for Solar-Village site, Saudi Arabia.

1563

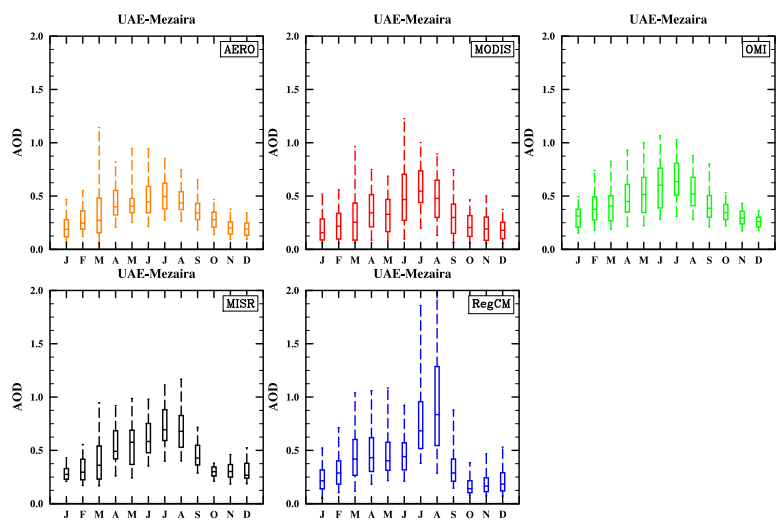


Figure 6. The AOD annual cycle statistics as in Fig. 4 but for Mezaira (UAE) site.

1564

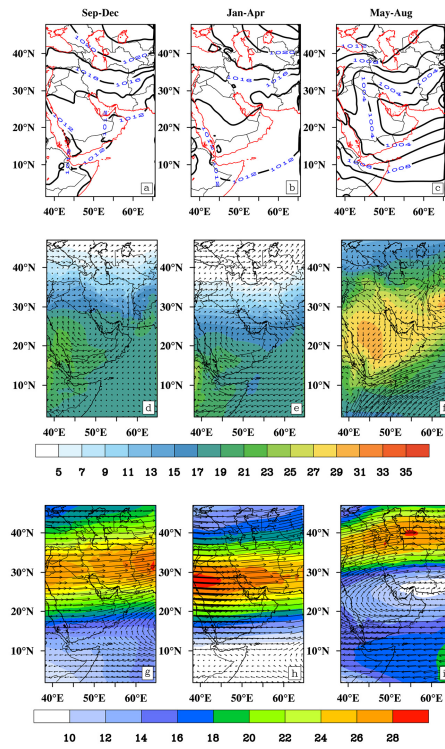


Figure 7. (a–c) The climatology (seasonal average) of the modeled mean sea level pressure in hPa, (d–f) the modeled 850 hPa Temperature in °C (shaded colors) and wind field (represented by vectors), (g–h) the modeled 200 hPa wind speed in ms^{-1} (shaded colors) and wind field (represented by vectors). All data is based on the 2000–2012 time interval.

1565

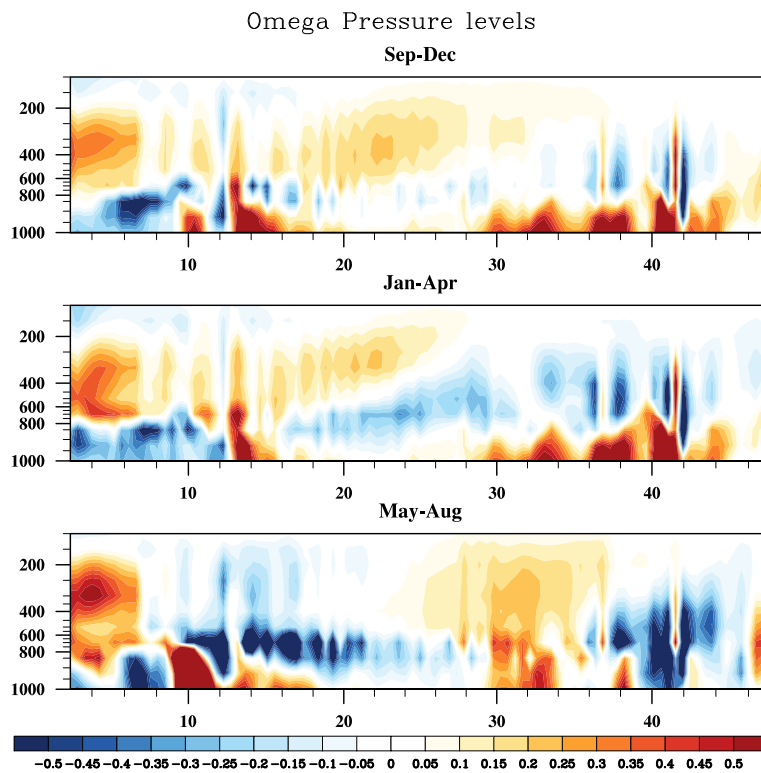


Figure 8. Climatology (seasonal average) of vertical velocity zonally averaged (averaged from 36 to 45° E and based on 2000–2012 time interval). The color scale represents vertical velocity in hPa s^{-1} . The x axis is latitude and y axis is pressure level in hPa.

1566

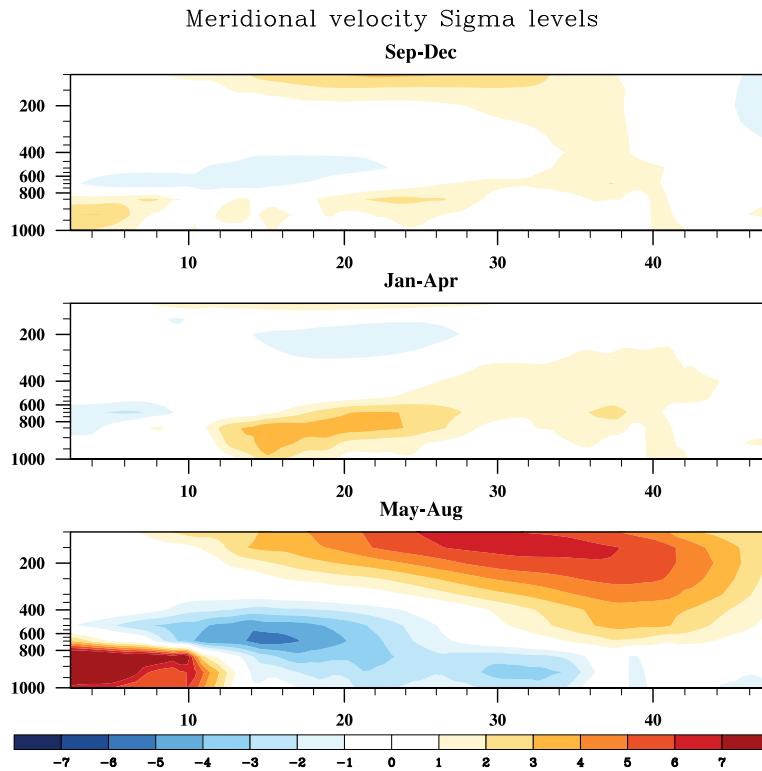


Figure 9. Climatology (seasonal average) of meridional velocity zonally averaged (averaged from 36 to 50° E and based on 2000–2012 time interval). The color scale represents velocity in ms^{-1} . The x axis is latitude and y axis is pressure level in hPa.

1567

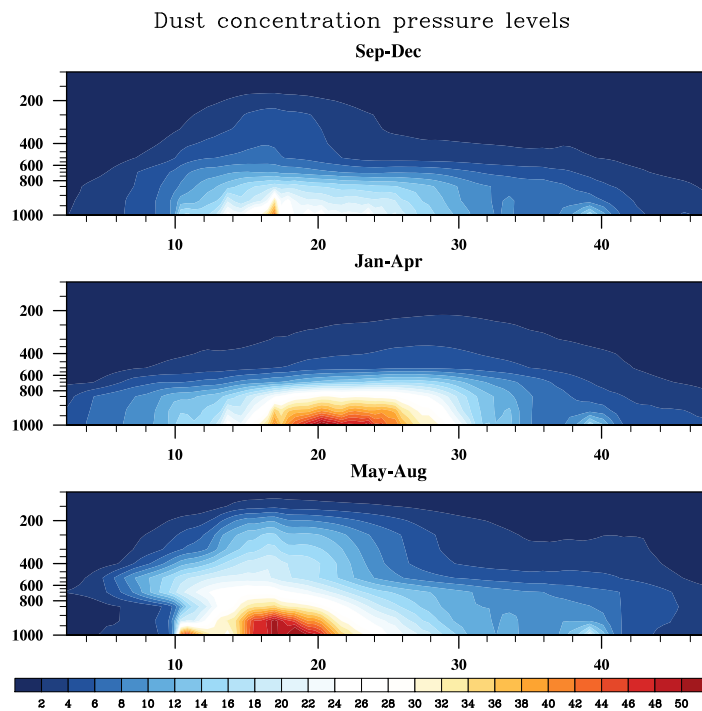


Figure 10. Climatology (seasonal average) of fine dust ($0.01\text{--}1\ \mu\text{m}$) concentration in $\mu\text{g m}^{-3}$ zonally averaged (averaged from 36 to 50° E and based on 2000–2012 time interval). The color scale represents concentration in $\mu\text{g m}^{-3}$. The x axis is latitude and y axis is pressure level in hPa.

1568

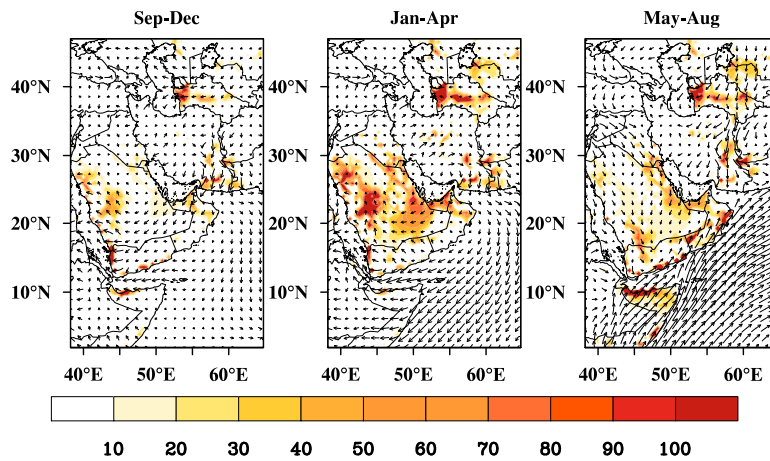


Figure 11. Climatology (seasonal average) of surface fine ($0.01\text{--}1\ \mu\text{m}$) dust emission flux for fine dust ($\text{mg m}^{-2} \text{day}^{-1}$) based on 2000–2012 interval.

1569

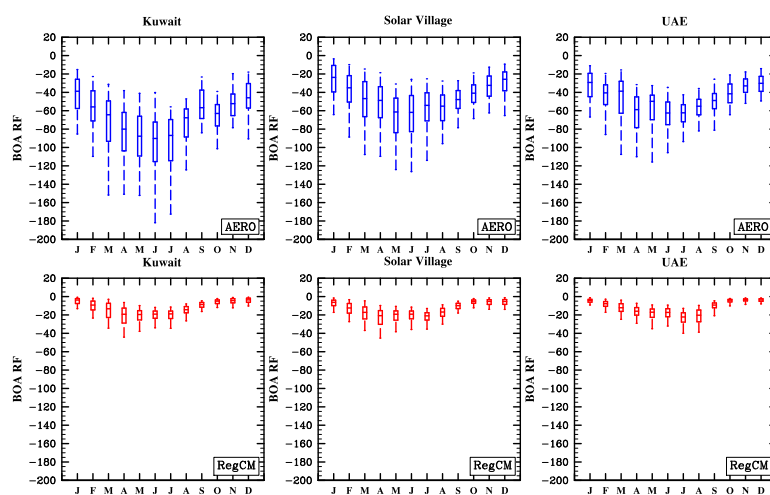


Figure 12. The Bottom of Atmosphere radiative forcing of (BOARF) AERONET inversion products (blue) and the RegCM4 output (red), spatially averaged around the AERONET sites.

1570

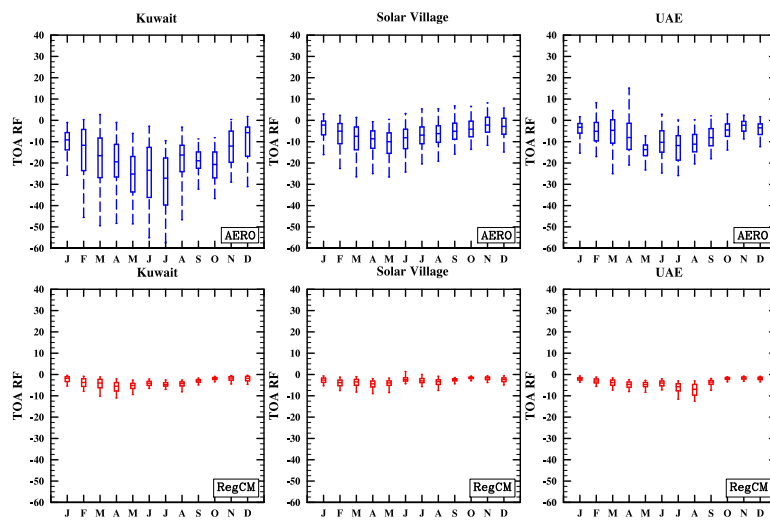


Figure 13. The Top of Atmosphere radiative forcing (TOARF) of AERONET inversion products (blue) and the RegCM4 output (red), spatially averaged around the AERONET sites.